

Hydrodynamic investigation of a dual-chamber OWC Wave Energy Converter

De-Zhi Ning, Rong-Quan Wang, Ying Gou

State Key Laboratory of Coastal and Offshore Engineering, Dalian University of Technology, Dalian, 116024, China

Email: dzning@dlut.edu.cn

1. Introduction

The OWC device becomes one of the most favorable wave energy converters for its high efficiency and structural simplicity. In the recent decades, a great volume of researches have been carried out to investigate the hydrodynamic performance of single-chamber OWC. Generally, for a single-chamber OWC, it has been recognized that the device is to be an efficient absorber only when it operates at near-resonance (Falcão, 2002; Iturrioz et al., 2015). To enhance the performance of the OWC devices, the multi-chamber OWC concept has been proposed. Rezanejad et al., (2013, 2015) analytically and numerically studied the hydrodynamic efficiency of a dual-chamber OWC placed over stepped bottom. Ning et al., (2017) numerically investigated the performance of a dual-chamber OWC device, which has two sub-chambers with a shared orifice.

As an extension of the authors' previous work (Ning et al., 2016, 2017), the present abstract considers a fixed OWC wave energy device with two independent sub-chambers. The hydrodynamic efficiency of the proposed OWC device is compared with the single-chamber device. The hydrodynamic efficiency, free surface elevations and air pressures in the two sub-chambers are investigated experimentally and numerically.

2. Experimental and numerical models

2.1 Experimental setup

The physical model tests are carried out in the wave-current flume at Dalian University of Technology. The wave-current flume is 69 m long, 2 m wide and 1.8 m deep. The OWC model is installed at a position 50 m away from the wave maker.

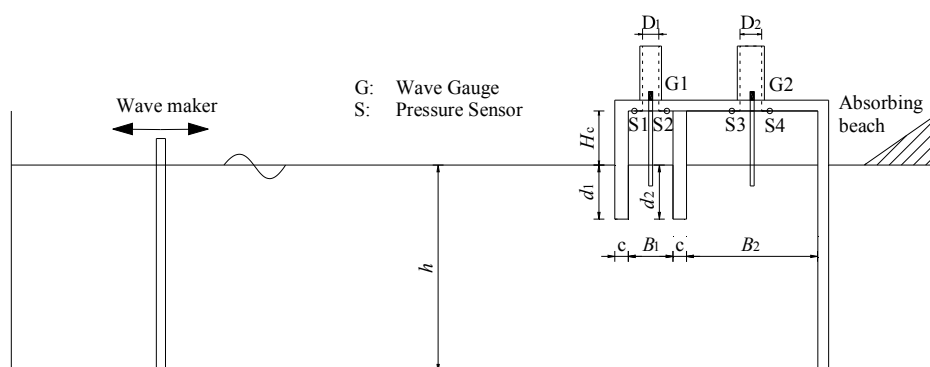


Fig. 1 Schematic of the experimental setup.

The schematic of the experimental setup is shown in Fig.1. The following parameters are given in the experiments, i.e., water depth $h=1.0\text{m}$, barrier wall thickness $C=0.05\text{ m}$, barrier wall drafts $d_1=d_2=0.125\text{ m}$, chamber height $H_c=0.20\text{ m}$. By keeping the total chamber width constant (i.e., $B_1+B_2+C=0.70\text{ m}$), three different widths of the two chambers ($B_1: B_2=3:1, 1:1, 1:3$) are examined. Two circular orifices on the roof of each chamber are used to simulate the power take-off (PTO) mechanism and the area ratio of the orifices are both kept 0.66%. Two resistance-type wave gauges

are used to measure the instantaneous surface elevations at different positions (i.e., G1 and G2). Each chamber is set two pressure sensors to measure the air pressure. Both the surface and air pressure sensors are sampled at 50 Hz. The incident wave amplitude A_i is 0.03 m and wave periods T is in the scope of (1.0 s, 2.3 s).

2.2 Numerical model

Under the assumption of the ideal fluid, a 2D fully nonlinear numerical model is developed to model the OWC device based on potential flow theory and higher-order boundary element method (HOBEM). The incident wave is generated by the inner-domain sources, the governing equation is described with Poisson equation and a damping layer with a coefficient $\mu_1(x)$ at the left end of the numerical flume is applied to absorb the reflected wave from the device. Then, velocity potential satisfies the following fully nonlinear free surface boundary conditions

$$\begin{cases} \frac{dX(x, z)}{dt} = \nabla \phi - \mu_1(x)(X - X_0) \\ \frac{d\phi}{dt} = -g\eta + \frac{1}{2}|\nabla \phi|^2 - \frac{p_a}{\rho} - \mu_1(x)\phi \end{cases}, \quad (1)$$

where $X_0=(x_0, 0)$ denotes the initial static position of the fluid particle. The definition of damping coefficient $\mu_1(x)$ can refer to Ning et al.(2008).

Outside of the chamber, the air pressure p_a on the water free surface is set to be zero (i.e., atmospheric pressure), while inside the chamber, the pneumatic pressure is specified on the free-surface:

$$p_a(t) = D_{dm} |U_d(t)| U_d(t), \quad (2)$$

where D_{dm} is quadric pneumatic damping coefficient and $U_d(t)$ the air flow velocity in the orifice.

The captured wave energy from the OWC device in the numerical model can be calculated by

$$P_{0i} = \frac{1}{T} \int_t^{t+T} Q_i(t) p_{ai}(t) dt = \frac{1}{T} \int_t^{t+T} B \bar{\eta}_i(t) p_{ai}(t) dt = \frac{1}{T} \int_t^{t+T} D_{dm} |U_{di}(t)| U_{di}(t) A U_{di}(t) dt, \quad (3)$$

where the flow rate Q_i , $\bar{\eta}_i$ is the time mean vertical velocity of the free surface inside the chamber. Then, the hydrodynamic efficiency of one chamber is defined as

$$\xi_i = \frac{P_{0i}}{P_{inc}} (i = 1, 2). \quad (4)$$

where P_{inc} is incident wave power. Then the total efficiency of the device is $\xi = \xi_1 + \xi_2$.

2. Results and discussions

In the numerical model, the length of the numerical flume is set to 5λ (where λ is wave length), in which 1.5λ at the left side is used as the damping layer; and the spatial step and temporal step are set as $\Delta x = \lambda/30$ and $\Delta t = T/80$ after convergent tests, respectively; the quadric pneumatic damping coefficient is set as $D_{dm} = 1.0$. The geometrical parameters are kept the same as in the experiments. For each case, 30 periods of waves are simulated.

The comparison between the experiments and simulations are carried out by choosing the two chamber widths to be $B_1 = B_2 = 0.325$ m (i.e. $B_1 : B_2 = 1 : 1$). Fig. 2 (a) and (b) show the time series of the predicted and observed free surface elevation at two sub-chambers center (i.e., G1 and G2) and

the air pressure in the two sub-chambers with $T = 1.5$ s, respectively. Fig. 3 (a) and (b) show the predicted and observed non-dimensional maximum surface elevations and air pressures versus non-dimensional wave frequency kh (where k is the wave number), respectively. Good agreements between the numerical results and measurements are observed, which indicates that the present numerical model can simulate the interaction of water and air inside the chamber well. Fig. 3 shows that both the surface elevations and air pressures in the two chambers decrease with kh overall. The surface elevations and the air pressures in chamber 2 show the relative larger values than those in chamber 1 when $kh < 3.2$.

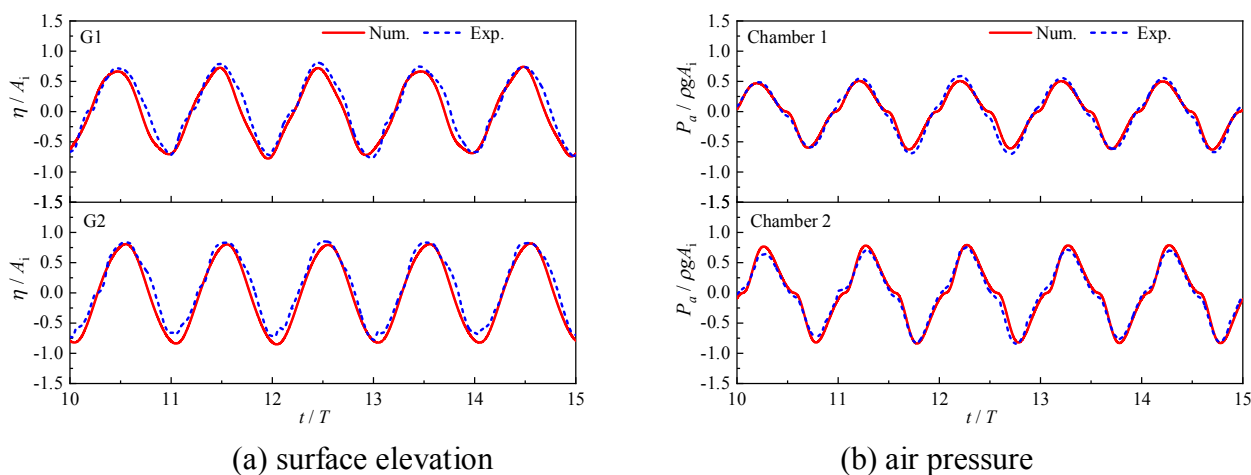


Fig. 2 Time series of the predicted and observed (a) free surface elevations at the chamber center and (b) air pressures in the chamber with $T = 1.5$ s ($B_1 = B_2 = 0.325$ m, $d_1 = d_2 = 0.125$ m).

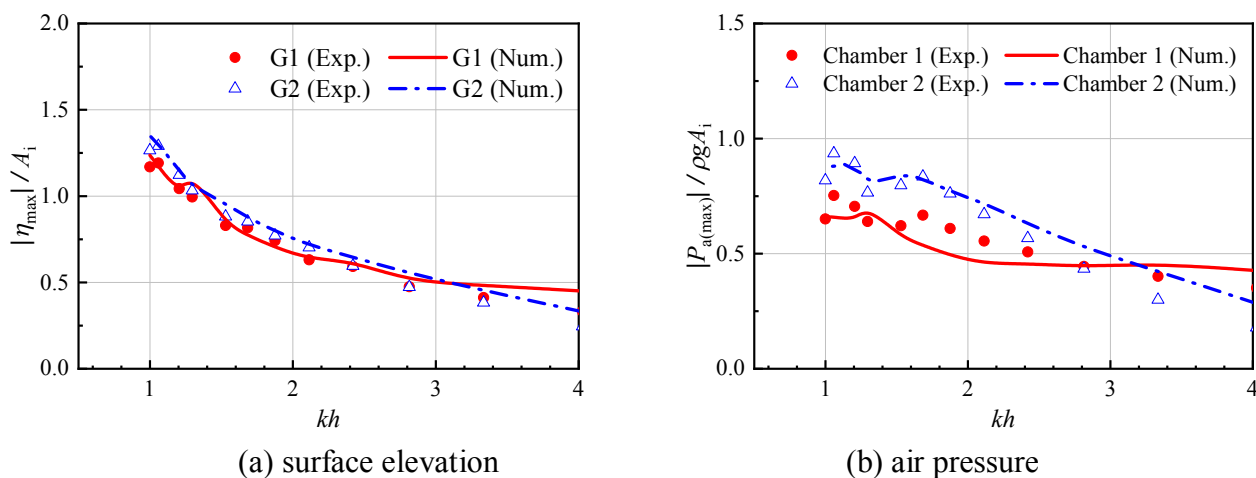


Fig. 3 Comparison of the maximum (a) surface elevations and (b) air pressures in the two sub-chambers ($B_1 = B_2 = 0.325$ m, $d_1 = d_2 = 0.125$ m).

The comparison of the hydrodynamic efficiency of two sub-chambers is shown in Fig. 4. The efficiency in chamber 2 increases firstly to a peak value and then decreases with the increase of kh . In chamber 1, the efficiency remains relatively stable and is lower than that in chamber 2 when kh is smaller than 3.2. However, in the high frequency region (i.e., $kh > 3.2$), the efficiency in chamber 1 is larger than that in chamber 2, which enhances the performance of the device for high frequency waves.

Fig. 5 shows the comparison of the efficiencies between dual-chamber and single chamber devices (i.e., chamber width $B = 0.70$ m and barrier wall draft $d = 0.14$ m (Ning et al., 2016)). The efficiency

of the dual-chamber device is larger than that of the single chamber. And the dual-chamber device broadens the effective frequency bandwidth. The effects of the chamber width on the total hydrodynamic efficiency of the dual chamber are also shown in Fig. 5.

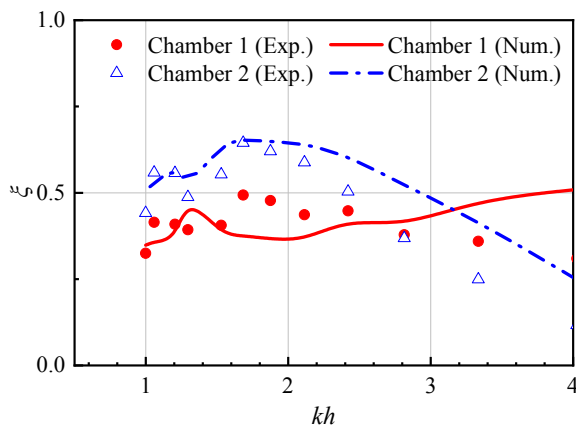


Fig. 4 Comparison of the hydrodynamic efficiency of the two sub-chambers ($B_1 = B_2 = 0.325$ m, $d_1 = d_2 = 0.125$ m).

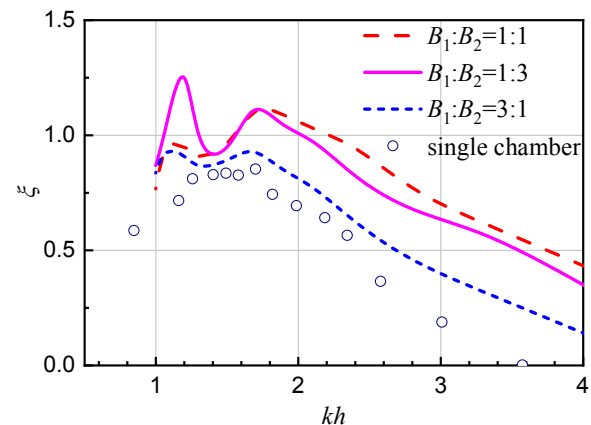


Fig. 5 Effects of the chamber width on the total hydrodynamic efficiency ($d_1 = d_2 = 0.125$ m).

3. Conclusions

The hydrodynamic performance of a dual-chamber OWC device is investigated experimentally and numerically in this study. It is found that the dual-chamber OWC device broadens the effective frequency bandwidth and performs better than the single-chamber device. More examples and further investigation on the wave-interaction with a dual-chamber OWC device will be presented at the workshop.

Acknowledgements

The authors would like to acknowledge financial support from the NSFC (Grant No. 51679036) and the UK-China Industry Academia Partnership Programme (Grant No. UK-CIAPP\73).

References

- Falcão, A.F.D., 2002. Wave-power absorption by a periodic linear array of oscillating water columns. *Ocean Engineering* 29 (10), 1163-1186.
- Iturrioz, A., Guanche, R., Lara, J.L., Vidal, C., Losada, I.J., 2015. Validation of OpenFOAM® for Oscillating Water Column three-dimensional modeling. *Ocean Engineering* 107, 222-236.
- Ning, D., Wang, R., Zhang, C., 2017. Numerical Simulation of a Dual-Chamber Oscillating Water Column Wave Energy Converter. *Sustainability* 9 (9), 1599.
- Ning, D.Z., Teng, B., Eatock Taylor, R., Zang, J., 2008. Numerical simulation of non-linear regular and focused waves in an infinite water-depth. *Ocean Engineering* 35 (8-9), 887-899.
- Ning, D.Z., Wang, R.Q., Teng, B., Zang J., Chen L.F., 2016. Hydrodynamic investigation of a fixed OWC Wave Energy Converter. 31th IWWFEB, 3-6 April, Plymouth MI, USA.
- Rezanejad, K., Bhattacharjee, J., Soares, C.G., 2013. Analytical and Numerical Study of Nearshore Multiple Oscillating Water Columns, Proceedings of the Asme 32nd International Conference on Ocean, Offshore and Arctic Engineering, Nantes, France.
- Rezanejad, K., Bhattacharjee, J., Soares, C.G., 2015. Analytical and numerical study of dual-chamber oscillating water columns on stepped bottom. *Renewable Energy* 75, 272-282.